Supplementary Information

Surface engineering of nanoflower-like MoS_2 decorated porous Si_3N_4 ceramics for electromagnetic wave absorption

Jialin Bai,[ab] Shijie Huang,[ab] Xiumin Yao,*[a] Xuejian Liu*[a] and Zhengren Huang*[a]

[a] State Key Laboratory of High Performance Ceramics and Superfine Microstructures, Shanghai Institute of Ceramics, Chinese Academy of Sciences, Shanghai 200050, China

[b] Center of Materials Science and Optoelectronic Engineering, University of Chinese Academy of Sciences, Beijing 100049, China

* Corresponding Authors: xmyao@mail.sic.ac.cn (Xiumin Yao), xjliu@mail.sic.ac.cn (Xuejian Liu), zhrhuang@mail.sic.ac.cn (Zhengren Huang).

Materials and Characterization

Materials

Commercial Si_3N_4 powder was used as starting material. Y_2O_3 and Al_2O_3 were used as sintering additives. Mono-dispersed poly methyl methacrylate (PMMA, d_{50}=~30 μm) micro-balls were used as a pore-forming agent. Sodium molybdate dihydrate ($Na_2MoO_4 \cdot 2H_2O$) and thioacetamide (C_2H_5NS) were used for the synthesis of MoS_2. All chemicals were of analytical grade and were used as received without further purification.

Characterization

The phase composition of the samples was analyzed via X-ray diffraction (XRD, Cu Kα as radiation, Germany). The morphology of the fracture surface was observed using field emission scanning electron microscope (SEM, Hitachi SU8220, Japan) and transmission electron microscopy (TEM, JEM-2100F). Apparent porosity was measured by the Archimedes method. The surface element composition and its chemical states were determined by X-ray photoelectron spectroscopy (XPS, Thermo Fisher Scientific ESCALAB 250). Raman spectra were obtained on a LabRam HR800 with a visible laser (532 nm) to characterize the structure of the samples. The vector network analyzer (VNA, Agilent E5071C; China) was carried out to test the complex permittivity of the samples with dimensions of 22.86 mm × 10.16 mm × 3 mm in the frequency range of 8.2-12.4 GHz.

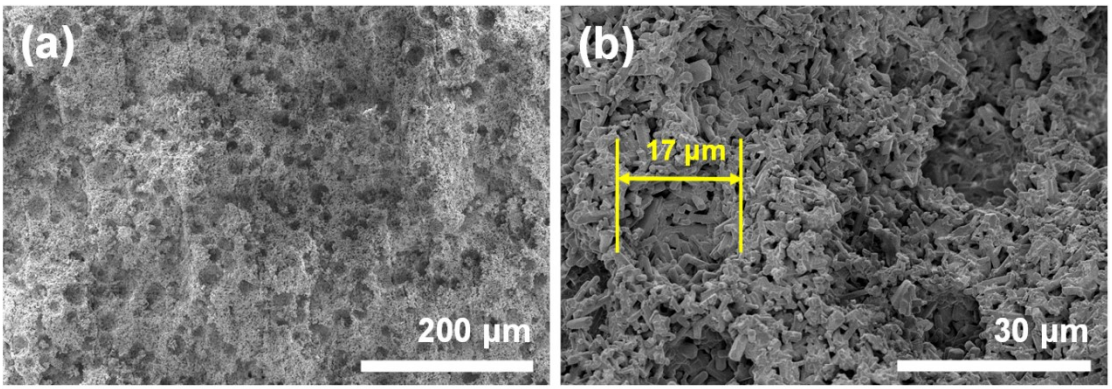

Figure S1. The fracture surfaces of porous Si_3N_4 ceramic.

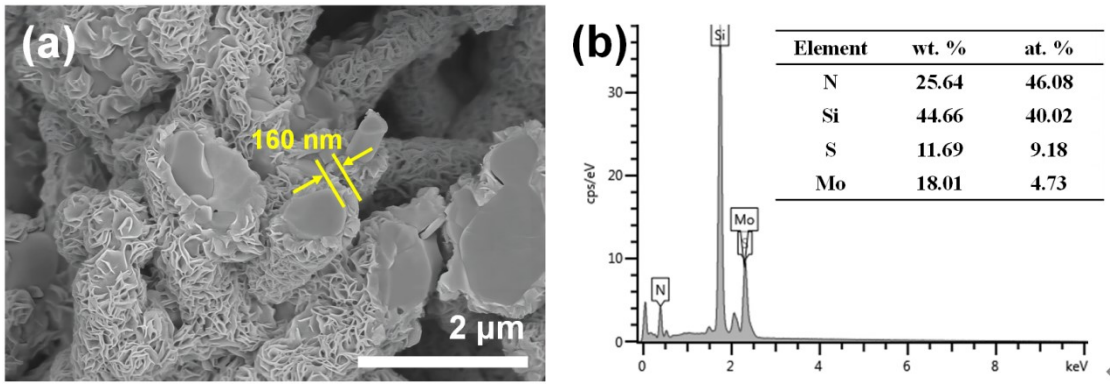

Figure S2. (a) The fracture surface and (b) EDS results of MoS_2/Si_3N_4-1.70.

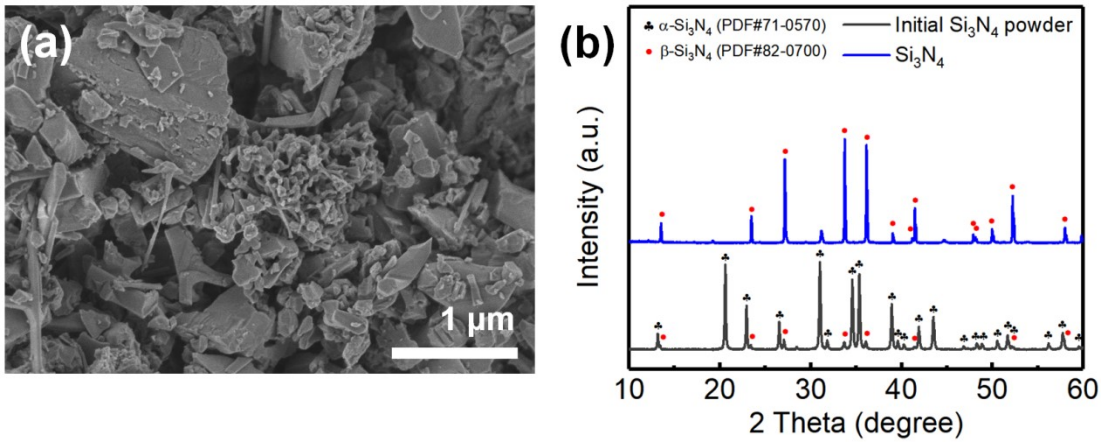

Figure S3. (a) The microstructure of initial Si_3N_4 powder. (b) XRD pattern of initial Si_3N_4 powder and porous Si_3N_4 ceramics.

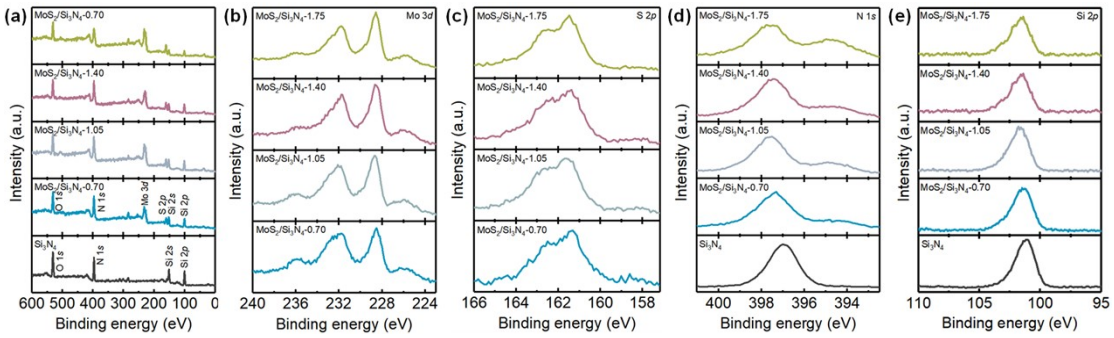

Figure S4. (a) XPS survey spectrum and high resolution XPS spectra of (b) Mo 3*d*, (c) S 2*p*, (d) N 1*s*, and (e) Si 2*p*.

Table S1. Summary of the average real part ($\varepsilon^{'}$), imaginary part ($\varepsilon^{''}$) of complex permittivity, and dielectric loss tangent ($\tan\delta_{\varepsilon}$) for different samples

Sample	$\varepsilon^{'}$	$\varepsilon^{''}$	$\tan\delta_{\varepsilon}$
MoS_2/Si_3N_4-0.70	3.52	0.92	0.26
MoS_2/Si_3N_4-1.05	3.82	1.94	0.51
MoS_2/Si_3N_4-1.40	4.64	2.69	0.58
MoS_2/Si_3N_4-1.75	5.72	3.64	0.64